Planar squeezing by quantum non-demolition measurement in cold atomic ensembles

2013 New J. Phys. 15 103031

(http://iopscience.iop.org/1367-2630/15/10/103031)

New Journal of Physics
The open access journal for physics

Planar squeezing by quantum non-demolition measurement in cold atomic ensembles

Graciana Puentes[1,3], **Giorgio Colangelo**[1], **Robert J Sewell**[1] **and Morgan W Mitchell**[1,2,3]

[1] ICFO—Institut de Ciencies Fotoniques, Mediterranean Technology Park, E-08860 Castelldefels, Barcelona, Spain
[2] ICREA—Institució Catalana de Recerca i Estudis Avançats, E-08015 Barcelona, Spain
E-mail: graciana.puentes@icfo.es and morgan.mitchell@icfo.es

New Journal of Physics **15** (2013) 103031 (14pp)
Received 5 May 2013
Published 28 October 2013
Online at http://www.njp.org/
doi:10.1088/1367-2630/15/10/103031

Abstract. Planar squeezed states, i.e. quantum states which are squeezed in two orthogonal spin components, have recently attracted attention due to their applications in atomic interferometry and quantum information (He *et al* 2012 *New J. Phys.* **14** 093012). While canonical variables such as quadratures of the radiation field can be squeezed in at most one component, simultaneous squeezing in two orthogonal spin components can be achieved due to the angular momentum commutation relations. We present a novel scheme for planar squeezing via quantum non-demolition (QND) measurements in spin-1 systems. The QND measurement is achieved via near-resonant paramagnetic Faraday rotation probing, and the planar squeezing is obtained by sequential QND measurement of two orthogonal spin components. We compute the achievable squeezing for a variety of optical depths, initial conditions and probing strategies. The planar squeezed states generated in this way contain entanglement detectable

[3] Authors to whom any correspondence should be addressed.

by spin-squeezing inequalities and give an advantage relative to non-squeezed states for any precession phase angle, a benefit for single-shot and high-bandwidth magnetometry.

Contents

1. Introduction

Quantum squeezing, the reduction of uncertainty in quantum observables below 'classical' or standard quantum limits (SQLs) [1–3], is an area of active research with applications in quantum information processing [4–8], quantum communications [9–11] and quantum metrology [12–14]. Here we consider a practical, measurement-based strategy to produce a new kind of squeezing in atomic spin ensembles. By way of introduction, we note that a spin **F** obeys the spin uncertainty relations

$$\Delta F_z \Delta F_x \geqslant \tfrac{1}{2}|\langle F_y\rangle| \tag{1}$$

and permutations (throughout we take $\hbar = 1$). These are distinctly different from the Heisenberg relation $\Delta X \Delta P \geqslant \frac{1}{2}$ that governs canonical variables X, P [15]. For canonical variables, the constant right-hand side (rhs) of the Heisenberg relation implies that reduction of the variance in one quadrature inevitably increases the variance of the other. In contrast, in spin systems the rhs of the uncertainty relation may vanish, e.g. if $\langle F_y\rangle = 0$, with the consequence that two spin components, e.g. F_z and F_x, may be *simultaneously* squeezed, with the uncertainty being absorbed by the third component. We note that this is subtly different from the Einstein–Podolsky–Rosen (EPR) entangled state studied in [16] where the sum and difference of canonical variables of two different spin systems were simultaneously squeezed. An analogous situation involving the Stokes parameters of light, which themselves obey angular momentum commutation relations, has also been studied [17–19]. For atomic spin ensembles, the suggestion of 'intelligent' spin states [20] predates even the concept of optical squeezing, and *planar quantum squeezing* (PQS) has recently been analyzed and proposed for quantum metrological applications [21, 22].

As described in [21, 22], PQS has the prospect of improving the precision of atomic interferometers at arbitrary phase angles, as it allows both orthogonal variances to be below the shot-noise level [23, 24]. This is opposed to squeezing on a single direction, which is only beneficial to refine the estimate of a phase angle already known with some precision

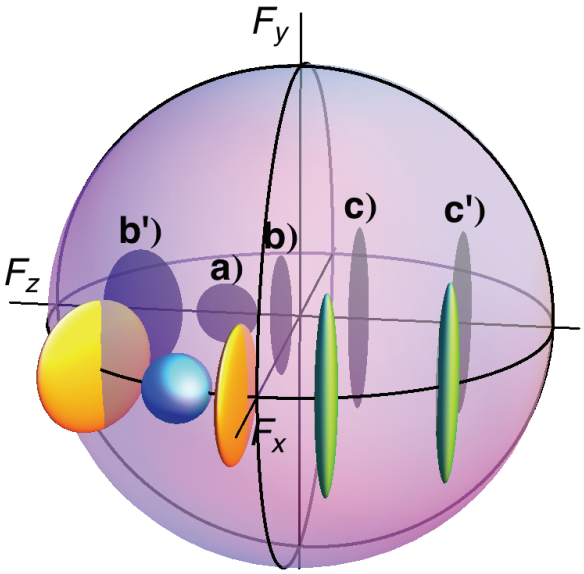

Figure 1. Illustration of spin variances for: (a) an unsqueezed state with SQL variances $\Delta^2 F_i$ for all components $i \in \{x, y, z\}$, (b), (b′) a state with squeezed azimuthal component. For measurements of F_z, this squeezing is advantageous only for certain precession angles, as in (b), but disadvantageous for others, as in (b′). (c), (c′) a planar squeezed state with both variances $\Delta^2 F_x$ and $\Delta^2 F_z$ reduced below the SQL is advantageous at all angles.

(see figure 1). High-bandwidth atomic magnetometry [25, 26], in which the precession angle may not be predictable in advance, would be a natural application. At the same time, there is interest in the entanglement properties of PQS states, which can be detected by spin-squeezing inequalities [21, 22, 27].

He *et al* [21] proposed an implementation of PQS using a two-well Bose condensate with tunable and attractive interactions. Here, we propose an alternative strategy in which the PQS state is prepared by sensitive [28] non-destructive [29] spin measurements. Sufficiently good measurements satisfy quantum non-demolition (QND) criteria [30] and produce (conditional) squeezing [14] of the measured spin variable. Stroboscopic probing a polarized ensemble of cold ^{87}Rb atoms, precessing in a constant external magnetic field, allows sequential measurement of two orthogonal components. As we show, this can squeeze two spin components simultaneously. We work with the collective total angular momentum variable $\mathbf{F}$ for spin-1 systems. The collective atomic spin is measured using paramagnetic Faraday rotation with an off-resonant probe. The ensemble of spins, polarized along a fixed direction by optical pumping, interacts with an optical pulse of duration τ and polarization described by the Stokes vector $\mathbf{S} = (S_x, S_y, S_z)$, through an effective Hamiltonian.

The paper is structured as follows: in section 2, we describe the formalism for light–atom interactions in polarized atomic ensembles and define spin-squeezing parameters. In section 3, we report numerical studies of PQS by QND measurement. In section 4, we discuss entanglement detection using spin-squeezing inequalities for the generated PQS states. In section 5 we provide an example for the applications of these ideas in high bandwidth (single shot) atomic magnetometry.

2. Atom–light interaction

Our modeling is based on covariance matrix techniques introduced by Madsen and Mølmer [31–33], extended to include inhomogeneities by Koschorreck and Mitchell [34], to three spin components by Toth and Mitchell [35] and to spin-1 atoms by Colangelo *et al* [36]. In brief, we consider a magnetic field $\mathbf{B}$ oriented along the y-axis, in interaction with a spin-1 ensemble, e.g. ^{87}Rb in the $F = 1$ ground state, and probed using Faraday rotation probing by near-resonant light pulses. The ensemble is described by collective spin observables, for example $\hat{F}_x \equiv \sum_i \hat{f}_x^{(i)}$, where $\hat{F}_x^{(i)}$ indicates the x-component of the spin of the ith atom. Here F_i correspond to the macroscopic magnetization components, which precess about the external magnetic field $\mathbf{B}$ at the Larmor frequency. Both spin orientation variables $\hat{F}_x$, $\hat{F}_y$, $\hat{F}_z$ and also spin alignment variables $\hat{J}_x$, $\hat{J}_y$, $\hat{J}_k$, $\hat{J}_l$, $\hat{J}_m$ defined using $\hat{j}_x \equiv \hat{f}_x^2 - \hat{f}_y^2$, $\hat{j}_y \equiv \hat{f}_x\hat{f}_y + \hat{f}_y\hat{f}_x$, $\hat{j}_k \equiv \hat{j}_k = \hat{f}_x\hat{f}_z + \hat{f}_z\hat{f}_x$, $\hat{j}_l = \hat{f}_y\hat{f}_z + \hat{f}_z\hat{f}_y$, $\hat{j}_m = \frac{1}{\sqrt{3}}(2\hat{f}_z^2 - \hat{f}_x^2 - \hat{f}_y^2)$, respectively, are required to describe the spin-1 system. The optical pulses are described in terms of Stokes operator components $\hat{S}_x$, $\hat{S}_y$, $\hat{S}_z$, defined as

$$\hat{S}_x \equiv \tfrac{1}{2}\hat{\mathbf{a}}^\dagger\boldsymbol{\sigma}_x\hat{\mathbf{a}}, \quad \hat{S}_y \equiv \tfrac{1}{2}\hat{\mathbf{a}}^\dagger\boldsymbol{\sigma}_y\hat{\mathbf{a}}, \quad \hat{S}_z \equiv \tfrac{1}{2}\hat{\mathbf{a}}^\dagger\boldsymbol{\sigma}_z\hat{\mathbf{a}}, \quad \hat{S}_0 \equiv \tfrac{1}{2}\hat{\mathbf{a}}^\dagger\mathbb{1}\hat{\mathbf{a}}, \tag{2}$$

where $\hat{\mathbf{a}} \equiv (\hat{a}_+, \hat{a}_-)^{\mathrm{T}}$ and $\hat{a}_+, \hat{a}_-$ are the annihilation operators for the left and right circular polarization, $\boldsymbol{\sigma}_x$, $\boldsymbol{\sigma}_y$, $\boldsymbol{\sigma}_z$ the Pauli matrices and $\mathbb{1}$ is the identity matrix. The $\hat{S}_x$, $\hat{S}_y$ and $\hat{S}_z$, $\hat{S}_0$ Stokes operators represent polarized light in the horizontal or vertical direction, polarized light in the $\pm 45^\circ$ direction, right-hand or left-hand circularly polarized light and the pulse energy respectively. As mentioned, they obey the same commutation relations as angular momentum operators.

The full computational machinery is described in detail in [36]. In brief, we use a phase-space vector to describe the state of the whole system

$$\hat{\mathbf{V}} = \mathbf{B} \oplus \hat{\mathbf{F}} \oplus \hat{\mathbf{J}} \oplus \bigoplus_{m=1}^{N_{\mathrm{pulses}}} \hat{\mathbf{S}}^{(m)}, \tag{3}$$

where $\oplus$ indicates the direct sum, the superscript $^{(m)}$ indicates the mth optical pulse and $\mathbf{B}$ is the magnetic field vector at the location of the ensemble. $\mathbf{B}$ is here a classical field, whereas the other components of $\hat{\mathbf{V}}$ are operators. We work within the Gaussian approximation, i.e. we assume that $\hat{\mathbf{V}}$ is fully characterized by its average $\langle\hat{\mathbf{V}}\rangle$ and by its covariance matrix Γ_{V}:

$$\Gamma_{\mathbf{V}} \equiv \tfrac{1}{2}\langle\hat{\mathbf{V}} \wedge \hat{\mathbf{V}} + (\hat{\mathbf{V}} \wedge \hat{\mathbf{V}})^{\mathrm{T}}\rangle - \langle\hat{\mathbf{V}}\rangle \wedge \langle\hat{\mathbf{V}}\rangle, \tag{4}$$

where $\wedge$ indicates the outer product. The phase space vector $\hat{\mathbf{V}}$ evolves under the effect of the Hamiltonian

$$H_{\mathrm{eff}} = -g_{\mathrm{F}}\mu_{\mathrm{B}}\mathbf{B}\cdot\hat{\mathbf{F}} + \frac{1}{\tau}[G_1\hat{S}_z\hat{F}_z + G_2(\hat{S}_x\hat{J}_x + \hat{S}_y\hat{J}_y + \frac{1}{\sqrt{3}}\hat{S}_0\hat{J}_m)], \tag{5}$$

where μ_{B} is the Bohr magneton and g_{F} is the gyromagnetic factor, τ is the pulse duration and $G_{1,2}$ are vectorial and tensorial coupling coefficients, respectively. Also included in the evolution are the decohering effects of incoherent scattering of probe photons and inhomogeneous magnetic fields [34].

The strategy to generate planar squeezing is illustrated in figure 2, and can be described as follows: an initial state is prepared and made to precess in the x–z plane by a magnetic field

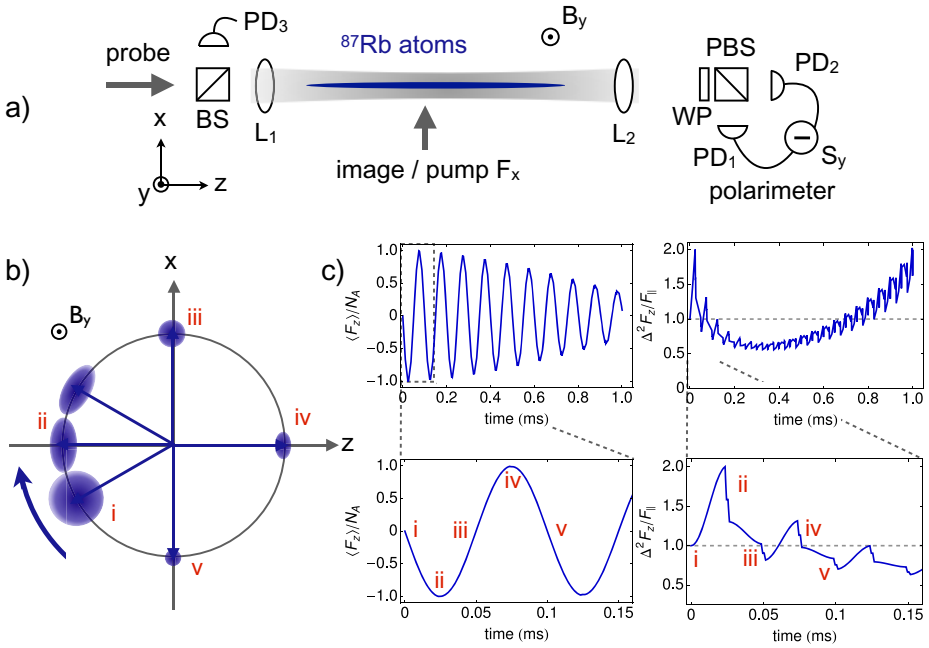

Figure 2. (a) Experimental setup. PD: photodiode; L: lens; WP: wave plate; BS: beam splitter; PBS: polarizing beam splitter. (b), (c) Planar squeezing is achieved by measuring the Faraday rotation of the Stokes components in the off-resonant probe light at four different moments during the Larmor precession cycle [37]. Each measurement consists of a pair of h- and v-polarized optical pulses and has a total duration of 3 μs, and produces a Faraday rotation signal proportional to the z-component of the collective atomic spin in the laboratory frame of reference at that phase of the 100 μs long Larmor precession cycle. In (b) we illustrate the measurement cycle: (i) a Poissonian coherent spin state (PCSS) is prepared and rotates in the x–z plane due to the applied magnetic field B_y. The first measurement (ii) squeezes the F_z component of the collective spin. The second measurement (iii) squeezes the F_x component of the collective spin, which is now aligned along the z-axis of the laboratory frame. The two measurements are repeated at moments (iv) and (v), further squeezing the F_z and F_x components of the collective atomic spin. The evolution of the average collective spin F_z and variance var(F_z) in the laboratory frame of reference during this measurement cycle is illustrated in (c). The top left panel shows the precession of the average F_z over multiple Larmor precession periods. The collective spin coherence decays due to scattering of photons during the measurements. The moment that the measurements (ii)–(v) are made is indicated in the bottom left panel, which shows a magnification of the first Larmor precession cycle. The evolution of the variance var(F_z) of the collective spin is shown in the top right panel. The sharp jumps are due to the measurement pulses, which squeeze the measured F_z component (in the laboratory frame). In between the pulses noise is rotated into the F_z component of the collective spin by the magnetic field. A magnification of the first Larmor precession cycle is shown in the bottom right panel. Pulses (ii) and (iv) squeeze the F_z component (in the atomic frame) and pulses (iii) and (v) squeeze the F_x component.

oriented along y (the $\mathbf{B}\cdot\hat{\mathbf{F}}$ term in $H_{\rm eff}$). Pulses of light, short on the time-scale of the precession, and with initial polarization along S_x, are sent through the ensemble at quarter-cycle intervals. Through the $\hat{S}_z\hat{F}_z$ term, the light–atom interaction rotates the polarization from S_x toward S_y by an angle proportional to $\hat{F}_z$. A measurement of S_y then gives an indirect measurement of F_z, reducing its uncertainty. If this measurement is sufficiently precise it leaves F_z squeezed. A quarter-cycle later, the state has precessed so that the F_x component can be measured, and possibly squeezed. The terms proportional to G_2 couple the orientation (F) components to the alignment (J) components, and for this application are simply an inconvenience. We suppress the effect of the G_2 term by dynamical decoupling, as described in [29].

While a given spin component can be squeezed by non-demolition measurement of that component, it is perhaps not obvious that planar squeezing, which requires simultaneous squeezing of non-commuting observables, should be producible by measurement. There is, after all, no projective measurement that indicates *both* F_x and F_z. Nevertheless, if $\langle F_y\rangle \approx 0$, the uncertainty relation of equation (1) does not impose a quantum back-action on F_x when F_z is measured, nor vice versa. This suggests that sequentially measuring F_x and F_z should squeeze both spin components and thus give planar squeezing.

The operational definition we adopt for planar squeezing follows the approach by He *et al* [21, 22], and can be summarized as follows. First, from equation (1) and permutations, we take $\Delta^2 F_x = \Delta^2 F_z = F_{||}/2$ as the SQL, where $F_{||} \equiv \sqrt{F_x^2 + F_z^2}$, so that $F_{||}$ is the magnitude of the in-plane spin components. Considering then the noise in the plane, we define the planar variance $\Delta^2 F_{||} \equiv \Delta^2 F_x + \Delta^2 F_z$, with SQL $\Delta^2 F_{||} = F_{||}$, and the *planar squeezing parameter*

$$\xi_{||}^2 \equiv \frac{\Delta^2 F_{||}}{F_{||}}. \tag{6}$$

A *planar squeezed state* has $\xi_{||}^2 < 1$, and also has individual component variances below the SQL, i.e. $\xi_x^2 < 1$, and $\xi_z^2 < 1$, where $\xi_i^2 \equiv 2\Delta^2 F_i/F_{||}$, so that $\xi_{||}^2 = (\xi_x^2 + \xi_z^2)/2$. We can also define a *metrological squeezing parameter* similar to the Wineland criterion [2] (see also equation (33) of *et al* [22])

$$\xi_{||,\mathrm{M}}^2 \equiv \frac{F\Delta^2 F_{||}}{F_{||}^2}, \tag{7}$$

where $F = \langle N_{\rm A}\rangle$ is the number of spins. A PQS state with $\xi_{||,M}^2 < 1$ gives enhanced metrological sensitivity to arbitrary phase shifts. In order to achieve this kind of state, it is convenient to have $\langle F_y\rangle = 0$ so that the uncertainties on the plane are only constrained by $\Delta F_x \Delta F_z \geqslant 0$. The uncertainty reduction in the two planar components comes at the expense of increasing the noise in the third component, as required by $\Delta F_{z(x)} \Delta F_y \geqslant \langle F_{x(z)}\rangle/2$.

3. Numerical results

We simulate an experiment illustrated in figure 2. An average of $\langle N_{\rm A}\rangle = 1.25 \times 10^6$ ^{87}Rb atoms are cooled in the $F = 1$ ground state and held in a weakly focused single beam optical dipole trap with an effective optical depth (OD) $\alpha_0 \approx 65$ [38]. To produce a PQS, we apply a magnetic field B_y to coherently rotate an initially F_x polarized coherent spin state in the x, z plane, and stroboscopically probe the spins at four times the Larmor frequency. We probe the atoms with μs pulses of linearly polarized off-resonant light detuned by $\Delta = -2\pi \times 10$ GHz on the D_2 line,

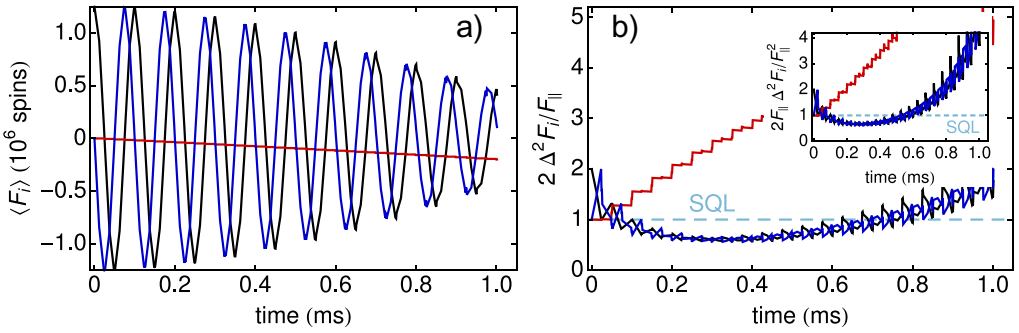

Figure 3. (a) Mean values of collective atomic angular momenta. Blue curve $\langle F_z \rangle$, black curve $\langle F_x \rangle$ and red curve $\langle F_y \rangle$. The mean value in the direction orthogonal to the plane of precession remains always approximately zero $\langle F_y \rangle \approx 0$, as required for planar squeezing. We note a reduction by roughly 10% in the mean collective atomic spins due to optical scattering. (b) Normalized variance of collective atomic spin components. Blue curve $2\Delta^2 F_z/F_{||}$, black curve $2\Delta^2 F_x/F_{||}$ and red curve $2\Delta^2 F_y/F_{||}$. As expected from the spin uncertainty relations, noise on the components in the (x, z)-plane are drop below the SQL $F_{||}/2$ indicated by the dashed line. In compensation, the out-of-plane variance $\Delta^2 F_y$ increases. The discontinuities in $\Delta^2 F_y$ correspond to probing events. Maximal planar squeezing is achieved at approximately 350 μs. The dashed blue line indicates the SQL. Inset: metrologically significant squeezing $2F\Delta^2 F_i/F_{||}^2$ for each component. Maximal sensitivity is achieved at approximately 300 μs.

detected by a shot-noise limited polarimeter. The pulses are sent through the atoms in pairs of alternating h- and v-polarization in order to cancel the effect of tensorial light shifts [29]. Each pulse is τ=1 μs long and contains 10^9 photons, and the two pulses in a pair are separated by 1 μs. Each stroboscopic measurement consists of a single pair of pulses with a total duration of 3 μs.

The coupling constant between the light and the atoms is $G_1 = 1.2 \times 10^{-8}$, calculated for this probe detuning using the experimental parameters described in [14]. The atomic ensemble is initially polarized in the x-direction by optical pumping, i.e. into a state $|+f_x\rangle^{\otimes N_A}$, where $|+f_x\rangle \equiv \frac{1}{2}(|m=-1\rangle + \sqrt{2}|m=0\rangle + |m=+1\rangle)$ and where N_A is subject to Poissonian fluctuations. This last condition is not imposed by quantum physics, which would allow N_A to be sharp, but rather represents the practical fact that trap loading is a stochastic process. We refer to this kind of state as a PCSS. The x-polarized PCSS has average values $\langle F_x \rangle = \langle N_A \rangle$, $\langle F_y \rangle = \langle F_z \rangle = 0$ and variances $\Delta^2 F_y = \Delta^2 F_z = \langle N_A \rangle/2$ (due to quantum fluctuations) and $\Delta^2 F_x = \langle N_A \rangle$ (due to ΔN_A). Further details of numerical simulations and the initial state are described in [36]. The external magnetic field along y, $B_y = 14.3$ mG, $B_x = B_z = 0$, produces Larmor precession in the (x, z)-plane, with a period of $T_L = 100$ μs, considerably longer than the $\sim$3 μs time required for the probing.

Results of numerical simulations for a typical condition are shown in figures 3 and 4. The ensemble of atoms is initially polarized in x-direction, and precesses in the (x, z)-plane due to the B-field at the Larmor frequency. As shown in figure 3(a), the mean value of the out-of-plane component remains near zero, i.e. $\langle F_y \rangle \ll \langle N_A \rangle$, so that the relevant uncertainty relation is $\Delta F_x \Delta F_z \geqslant |\langle F_y \rangle|/2$ imposes little back-action and the uncertainties in the (x, z) plane can be

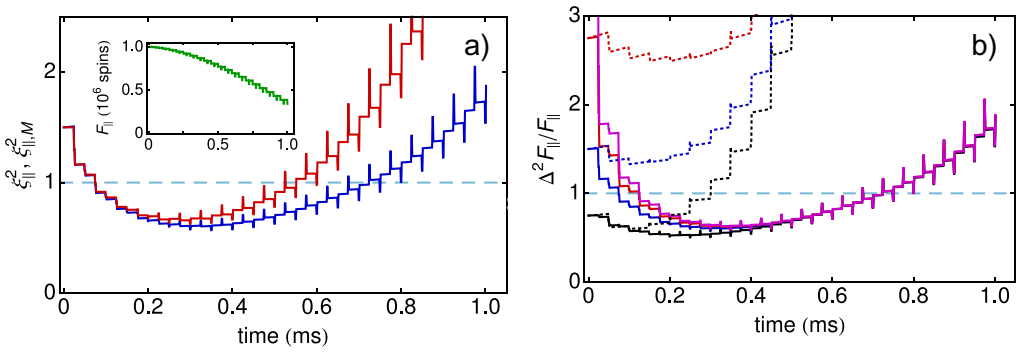

Figure 4. (a) Planar squeezing parameter $\xi_{||}^2 \equiv \Delta^2 F_{||}/F_{||}$ (blue curve) and metrological squeezing parameter $\xi_{||,\mathrm{M}}^2 \equiv F\Delta^2 F_{||}/F_{||}^2$ (red curve) during probing sequence. $\xi_{||}^2$ is reduced in steps due to stroboscopic probing and drops below unity, indicating planar squeezing. Maximal planar squeezing is achieved at approximately 350 μs and is reduced at longer times due to loss of atomic polarization by optical scattering. Maximal metrological sensitivity is achieved at approximately 300 μs. Inset shows the spin magnitude $F_{||}$, which is reduced by 10% during the total measurement time. (b) Planar squeezing parameter $\xi_{||}^2$ during probing for different initial states and different measurement strategies. Dashed lines show stroboscopic probing on a single component ($F_z, -F_z$ or two probing events per Larmor period), and solid lines show stroboscopic measurement on two components ($F_z, F_x, -F_z, -F_x$ or four events). Black, blue, red and magenta curves correspond to different variances in atom number $\Delta^2 N_\mathrm{A} = x^2\langle N_\mathrm{A}\rangle$, $x = 1/2$, 1, 3/2 and 2, respectively. For the larger initial noise levels (blue, red and magenta curves) planar squeezing ($\xi_{||}^2 < 1$) can be achieved by probing both $\pm F_x$ and $\pm F_z$ (solid curves) but not by probing only $\pm F_z$ (dashed curves). In both panels the light-blue dashed line indicates the SQL.

simultaneously reduced. The observed deviation from $\langle F_y\rangle = 0$ is due to residual effects of the tensorial coupling term $G_2(\hat{S}_x\hat{J}_x + \hat{S}_y\hat{J}_y + +\frac{1}{\sqrt{3}}\hat{S}_0\hat{J}_m)$ in the effective Hamiltonian.

Figure 3(b) shows the variances of the spin components during the probing procedure. Because the initial state is a $F = 1$ PCSS, the individual (x, z) variances are initially unequal, but quickly take on similar values through measurement. They oscillate as a consequence of the Larmor precession, and are sequentially reduced due to the stroboscopic probing, which can be seen in the step-like jumps in the various curves. At the same time, the variance in the orthogonal direction $\Delta^2 F_y$ increases well above the SQL, as expected for a PQS state.

Figure 4(a) shows the planar squeezing parameter $\xi_{||}^2$, which drops below unity indicating the production of planar squeezing by QND measurement.

3.1. Two-spin-component measurement-induced squeezing

The optimal measurement strategy will depend in general on the amount of initial quantum and technical noise in the angular momentum components $\Delta F_i(t = 0)$, with $i = (x, z)$. If the initial noise in one component is sufficiently low (variance below $\langle N_\mathrm{A}\rangle$), then it may be enough to squeeze the remaining component by probing in a single direction. However, in most realistic

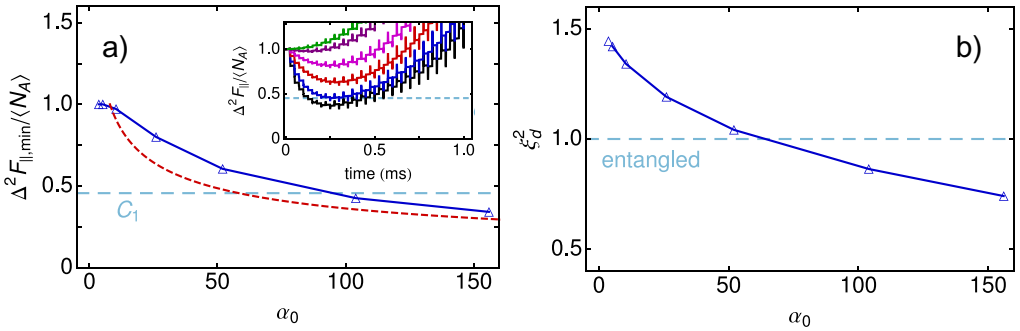

Figure 5. Spin squeezing and entanglement of PQS. (a) Entanglement detection in planar squeezing using the separability criterion $\Delta^2 F_{||}/\langle N_A\rangle \geqslant C_F$ of He *et al* [21], for which $C_1 = 7/16$ (light blue dashed line). Inset shows $\Delta^2 F_{||}/\langle N_A\rangle$ versus time for $\alpha_0 = 5$ (green), 10 (purple), 25 (magenta), 50 (red), 100 (blue) and 150 (black). Main graph shows minimal values achieved $\Delta^2 F_{\|,\min}$ versus α_0 (blue symbols). Blue line is a guide to the eye. The criterion detects entanglement for $\alpha_0 \gtrsim 100$. Dashed red line: simple estimate of planar squeezing parameter $\xi^2_{||,\min}$, for optimal spontaneous emission probability $\eta_0 = 1/\sqrt{2\alpha_0}$, see section 3.2. (b) The spin squeezing parameter of equation (5*d*) of [27] detects entanglement for $\xi_d^2 < 1$ (see equation (9)). The boundary is indicated by the light blue dashed line. Again, we plot the minimal values achieved versus α_0 for the curves in the inset of (a). This criterion detects entanglement for $\alpha_0 \gtrsim 60$.

scenarios it is preferable to probe the two in-plane components, so the noise of each can be reduced. Figure 4(b) shows the development of planar squeezing for one-component and two-component measurement strategies for different initial noise conditions.

3.2. Achievable squeezing versus optical depth

In the absence of scattering noise and decoherence, a QND measurement reduces the variance of the measured parameter by a factor $1/(1+\kappa)$, where κ is the signal-to-noise ratio of the measurement, proportional to the number of photons used in the measurement. At the same time, spontaneous scattering events add noise (variance) and reduce $F_{||}$, by amounts approximately linear in the number of photons used. An often-used estimate of the trade-off between these effects [31, 32] finds a minimum squeezing parameter $\xi^2 = 1/(1+\alpha_0\eta)+2\eta$, where η is the probability for any given atom to suffer a spontaneous emission event. This expression has a minimum $\xi^2_{\min} = 2\sqrt{(2/\alpha_0)}$ for the optimal η, which is $\eta_0 = 1/\sqrt{2\alpha_0}$. For a typical system with optical density $\alpha_0 \approx 25$ this optimal value gives a lower bound on the amount of squeezing given by roughly $\xi^2_{\min} \approx 0.5$ (3 dB of noise reduction) [39].

The predicted planar squeezing by this simple model is shown in figure 5(a) (red dashed line), for an OD ranging from $0 < \alpha \leqslant 150$. Also shown in figure 5(a) are full simulation results (inset), from which we can extract a more accurate estimate of the achievable planar squeezing, shown as blue symbols in the main graph. The difference at large α_0 (and thus large squeezing) may be attributable to finite precession angle between the h- and v-polarized parts of the probing. In the next section, we characterize the entanglement content of the generated planar squeezed states.

4. Spin squeezing inequalities and entanglement criteria

A number of spin-squeezing inequalities can in principle detect entanglement in planar squeezed states. He *et al* [21] give a simple inequality, obeyed by all separable states:

$$\frac{\Delta^2 F_{||}}{\langle N_{\rm A}\rangle} \geqslant C_F, \tag{8}$$

where $C_1 = 7/16$. As shown in figure 5(a), our procedure for producing planar squeezing can violate this inequality for ODs $\alpha_0 \gtrsim 35$.

A generalized spin squeezing parameter from Vitagliano *et al* [27] (equation 5(d))

$$\xi_d^2 \equiv \frac{(\langle N_{\rm A}\rangle - 1)[(\tilde{\Delta}F_x)^2 + (\tilde{\Delta}F_z)^2]}{\langle \tilde{F}_y^2\rangle - \langle N_{\rm A}\rangle(\langle N_{\rm A}\rangle - 1)F^2}, \tag{9}$$

where $\langle \tilde{F}_i^2\rangle \equiv \langle F_i^2\rangle - \langle \sum_n (f_i^{(n)})^2\rangle$ and $(\tilde{\Delta}F_i)^2 = (\Delta F_i)^2 - \langle \sum_n (f_i^{(n)})^2\rangle$ are modified second order moments and variances, also detects entanglement ($\xi_d^2 < 1$) in planar squeezed states, as shown in figure 5(b).

Regarding the difficulty of detecting entanglement in PQS states, we note a significant difference relative to one-component spin squeezing. With just one component, the border between squeezed and un-squeezed states coincides with the border between separable and entangled states. That is, a CSS is a pure product state and also has SQL noise. In contrast, by the planar squeezing criterion of He *et al* [22] (given as equation (6)) a CSS (with a definite $N_{\rm A}$), is already a planar squeezed state with $\xi_{||} < 1$. In this sense, planar squeezing is easier to achieve than entanglement.

5. Applications: optical magnetometry

We now describe a possible application of PQS in optical magnetometry, for determination of arbitrary angles with precision below the SQL. States that are squeezed in only one component can give a metrological advantage over a limited range of angles. Protocols to employ these states either require prior knowledge of the phase (enough to place them within the range of improved sensitivity), or adaptive procedures to determine the phase during the measurement. In contrast, planar squeezed states can give improved sensitivity for any precession angle [21, 22]. Here we show that QND-generated PQS states are effective for this purpose.

We have in mind a measurement scheme in which we initially prepare a PCSS in the x–z plane and measure for a few Larmor precession cycles, preparing a PQS state as described above. The PQS state is then allowed to freely evolve for as long as the coherence time of the state allows, before we again measure to determine the phase shift accumulated during this free evolution. The conditionally squeezed PQS state allows us to predict the outcome of the second measurement with a sensitivity better than the SQL for arbitrary cumulative phase shifts.

We consider a state, initially oriented in the F_x direction, and allowed to precess in response to a field $\mathbf{B}$ along the y-direction. The precession angle versus time t will be $\phi = \omega_{\rm L} t$, where $\omega_{\rm L}$ is the Larmor frequency, which in turn is proportional to B_y. After precession, the measured component F_z is

$$F_z^{(\rm out)} = F_x^{(\rm in)} \sin\phi + F_z^{(\rm in)} \cos\phi, \tag{10}$$

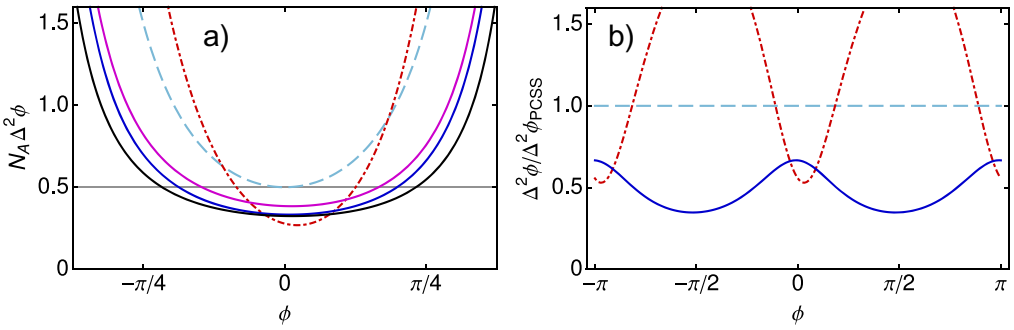

Figure 6. (a) Phase-estimation variance $\Delta^2\phi$ as a function of precession phase ϕ for planar squeezed states generated as described above. SQL $\Delta^2\phi = 1/(2\langle N_A\rangle)$ is indicated by the gray horizontal line, while curves show phase estimation uncertainty for various states. Black, blue and magenta solid curves show planar squeezed states generated as in figure 4(b) from coherent spin states with pre-squeezing number uncertainties $\Delta^2 N_A = x^2\langle N_A\rangle$, $x = 1/2$, 1 and 2, respectively. For such realistic PQS states, it is possible to reconstruct an arbitrary parameter with precision below the SQL within a significant interval of ϕ. The blue dashed curve shows the PCSS state. The red dot-dashed curve shows a SSS produced by probing only the F_z component of the atomic spin (blue dashed curve of figure 4(b)). This state has a ~60% reduction of the variance of the F_z component of the atomic spin, and a ~20% reduction of the collective spin coherence. It gives improved precision in a smaller region around the phase $\phi = 0$. The asymmetry of the PQS and SSS curves is a result of the non-zero $\mathrm{cov}(F_x, F_z)$ due to imperfect cancelation of tensorial light shifts during the measurement. (b) Comparison of phase estimation variance $\Delta^2\phi$ for a planar squeezed state (solid blue line), a single component squeezed state (dot-dashed red line), and the PCSS (light blue dashed line). States were generated by QND measurement as above. All curves are normalized to the PCSS value. A single component squeezed state can beat the precision of the PQS state for a few particular phases, but PQS states are more precise on average and offer an advantage relative to the PCSS for any phase.

where superscripts $^{(\mathrm{in})}$, $^{(\mathrm{out})}$ indicate the operators before and after the precession, respectively. We can calculate the uncertainty in ϕ as $\Delta^2\phi = \Delta^2 F_z^{(\mathrm{out})}/|\mathrm{d}\langle F_z^{(\mathrm{out})}\rangle/\mathrm{d}\phi|^2$ or, given that $\langle F_z^{(\mathrm{in})}\rangle = 0$,

$$\Delta^2\phi = \frac{\Delta^2 F(\phi)}{|F|^2\cos^2\phi}, \tag{11}$$

where $\Delta^2 F(\phi) \equiv \Delta^2 F_x^{(\mathrm{in})}\sin^2\phi + \Delta^2 F_z^{(\mathrm{in})}\cos^2\phi + \mathrm{cov}(F_x^{(\mathrm{in})}, F_z^{(\mathrm{in})})\sin 2\phi$, and $\mathrm{cov}(A, B) \equiv \frac{1}{2}\langle AB + BA\rangle - \langle A\rangle\langle B\rangle$ is the covariance. We note that PQS states reduce the planar variance for arbitrary angles on a finite interval, with the exception of the specific singular values which make the denominator in equation (11) equal to zero. This feature is depicted in figure 6(a), for realistic PQS states with different levels of technical noise, generated via QND measurements.

Figure 6(b) shows a comparison of the phase variances, relative to the PCSS. The results show that while a single-component squeezed state (SSS) is more precise than the PCSS (and

also the PQS) over a range of angles, the PQS gives a near-uniform advantage relative to the CSS and can be used for phase reconstruction below the SQL without prior knowledge of ϕ.

6. Conclusions

We have studied numerically the possibility to generate the recently proposed 'planar quantum squeezing', in which the variances of two orthogonal spin components are simultaneously squeezed, via quantum non-demolition measurement of cold atomic ensembles. We find that significant planar squeezing can be generated under realistic conditions and that this squeezing implies entanglement detectable with spin-squeezing inequalities. Considering the use of planar squeezed states in an optical magnetometry context, we find that planar squeezing can give a metrological advantage for estimation of arbitrary phase angles, whereas single-component spin squeezing is only advantageous for specific angle ranges. This is promising for high-bandwidth atomic magnetometry, in which a changing precession frequency may make it difficult or impossible to anticipate the precession phase.

Acknowledgments

The authors gratefully acknowledge Géza Tóth, Peter D Drummond and Giuseppe Vitagliano for fruitful discussions. They also would like to thank Naeimeh Behbood, Ferran Martin Ciurana and Mario Napolitano for helpful discussions. This work was supported by the Spanish MINECO under the project MAGO (ref. no. FIS2011-23520), by the European Research Council under the project AQUMET and by Fundació Privada Cellex. GP acknowledges financial support from Marie-Curie International Fellowship COFUND. All authors contributed equally to this work.

References

[1] Caves C M 1981 Quantum-mechanical noise in an interferometer *Phys. Rev.* D **23** 1693–708
[2] Wineland D J, Bollinger J J, Itano W M, Moore F L and Heinzen D J 1992 Spin squeezing and reduced quantum noise in spectroscopy *Phys. Rev.* A **46** R6797–800
[3] Kitagawa M and Ueda M 1993 Squeezed spin states *Phys. Rev.* A **47** 5138–43
[4] Braunstein S L and Pati A K 2010 *Quantum Information with Continuous Variables* (Berlin: Springer)
[5] Ourjoumtsev A, Tualle-Brouri R, Laurat J and Grangier P 2006 Generating optical Schrödinger kittens for quantum information processing *Science* **312** 83–6
[6] Dubost B, Koschorreck M, Napolitano M, Behbood N, Sewell R J and Mitchell M W 2012 Efficient quantification of non-Gaussian spin distributions *Phys. Rev. Lett.* **108** 183602
[7] Christensen S L, Béguin J B, Sørensen H L, Bookjans E, Oblak D, Müller J H, Appel J and Polzik E S 2013 Toward quantum state tomography of a single polariton state of an atomic ensemble *New J. Phys.* **15** 015002
[8] Beduini F A and Mitchell M W 2013 Optical spin squeezing: bright beams as high-flux entangled photon sources *Phys. Rev. Lett.* **111** 143601
[9] Vahlbruch H, Chelkowski S, Danzmann K and Schnabel R 2007 Quantum engineering of squeezed states for quantum communication and metrology *New J. Phys.* **9** 033602
[10] Appel J, Figueroa E, Korystov D, Lobino M and Lvovsky A I 2008 Quantum memory for squeezed light *Phys. Rev. Lett.* **100** 093602

[11] Usenko V C and Filip R 2011 Squeezed-state quantum key distribution upon imperfect reconciliation *New J. Phys.* **13** 113007
[12] Giovannetti V, Lloyd S and Maccone L 2004 Quantum-enhanced measurements: beating the standard quantum limit *Science* **306** 1330–6
[13] Wolfgramm F, Cerè A, Beduini F A, Predojević A, Koschorreck M and Mitchell M W 2010 Squeezed-light optical magnetometry *Phys. Rev. Lett.* **105** 053601
[14] Sewell R J, Koschorreck M, Napolitano M, Dubost B, Behbood N and Mitchell M W 2012 Magnetic sensitivity beyond the projection noise limit by spin squeezing *Phys. Rev. Lett.* **109** 253605
[15] Loudon R and Knight P L 1987 Squeezed light *J. Mod. Opt.* **34** 709–59
[16] Julsgaard B, Kozhekin A and Polzik E S 2001 Experimental long-lived entanglement of two macroscopic objects *Nature* **413** 400–3
[17] Korolkova N, Leuchs G, Loudon R, Ralph T C and Silberhorn C 2002 Polarization squeezing and continuous-variable polarization entanglement *Phys. Rev.* A **65** 052306
[18] Schnabel R, Bowen W P, Treps N, Ralph T C, Bachor H-A and Lam P K 2003 Stokes-operator-squeezed continuous-variable polarization states *Phys. Rev.* A **67** 012316
[19] Predojević A, Zhai Z, Caballero J M and Mitchell M W 2008 Rubidium resonant squeezed light from a diode-pumped optical parametric oscillator *Phys. Rev.* A **78** 63820
[20] Aragone C, Guerri G, Salamo S and Tani J L 1974 Intelligent spin states *J. Phys. A: Math. Nucl. Gen.* **7** L149
[21] He Q Y, Peng S G, Drummond P D and Reid M D 2011 Planar quantum squeezing and atom interferometry *Phys. Rev.* A **84** 022107
[22] He Q Y, Vaughan T G, Drummond P D and Reid M D 2012 Entanglement, number fluctuations and optimized interferometric phase measurement *New J. Phys.* **14** 093012
[23] Berry D W, Higgins B L, Bartlett S D, Mitchell M W, Pryde G J and Wiseman H M 2009 How to perform the most accurate possible phase measurements *Phys. Rev.* A **80** 052114
[24] Higgins B L, Berry D W, Bartlett S D, Mitchell M W, Wiseman H M and Pryde G J 2009 Demonstrating Heisenberg-limited unambiguous phase estimation without adaptive measurements *New J. Phys.* **11** 073023
[25] Shah V, Vasilakis G and Romalis M V 2010 High bandwidth atomic magnetometery with continuous quantum nondemolition measurements *Phys. Rev. Lett.* **104** 013601
[26] Vasilakis G, Shah V and Romalis M V 2011 Stroboscopic backaction evasion in a dense alkali-metal vapor *Phys. Rev. Lett.* **106** 143601
[27] Vitagliano G, Hyllus P, Egusquiza I L and Tóth G 2011 Spin squeezing inequalities for arbitrary spin *Phys. Rev. Lett.* **107** 240502
[28] Koschorreck M, Napolitano M, Dubost B and Mitchell M W 2010 Sub-projection-noise sensitivity in broadband atomic magnetometry *Phys. Rev. Lett.* **104** 093602
[29] Koschorreck M, Napolitano M, Dubost B and Mitchell M W 2010 Quantum nondemolition measurement of large-spin ensembles by dynamical decoupling *Phys. Rev. Lett.* **105** 093602
[30] Sewell R J, Napolitano M, Behbood N, Colangelo G and Mitchell M W 2013 Certified quantum non-demolition measurement of a macroscopic material system *Nature Photon.* **7** 517–20
[31] Madsen L B and Mølmer K 2004 Spin squeezing and precision probing with light and samples of atoms in the Gaussian description *Phys. Rev.* A **70** 052324
[32] de Echaniz S R, Mitchell M W, Kubasik M, Koschorreck M, Crepaz H, Eschner J and Polzik E S 2005 Conditions for spin squeezing in a cold ^{87}Rb ensemble *J. Opt. B: Quantum Semiclass. Opt.* **7** S548
[33] Mølmer K and Madsen L B 2004 Estimation of a classical parameter with Gaussian probes: magnetometry with collective atomic spins *Phys. Rev.* A **70** 052102
[34] Koschorreck M and Mitchell M W 2009 Unified description of inhomogeneities, dissipation and transport in quantum light–atom interfaces *J. Phys. B: At. Mol. Opt. Phys.* **42** 195502
[35] Tóth G and Mitchell M W 2010 Generation of macroscopic singlet states in atomic ensembles *New J. Phys.* **12** 053007

[36] Colangelo G, Sewell R J, Behbood N, Ciurana F M, Triginer G and Mitchell M W 2013 Quantum atom–light interfaces in the Gaussian description for spin-1 systems *New J. Phys.* **15** 103007

[37] Napolitano M, Koschorreck M, Dubost B, Behbood N, Sewell R J and Mitchell M W 2011 Interaction-based quantum metrology showing scaling beyond the Heisenberg limit *Nature* **471** 486–9

[38] Kubasik M, Koschorreck M, Napolitano M, de Echaniz S R, Crepaz H, Eschner J, Polzik E S and Mitchell M W 2009 Polarization-based light–atom quantum interface with an all-optical trap *Phys. Rev.* A **79** 043815

[39] Hammerer K, Mølmer K, Polzik E S and Cirac J I 2004 Light–matter quantum interface *Phys. Rev.* A **70** 044304